RESEARCH ARTICLE

Influence of Manganese and Copper Doping on Structural and Optical Properties of Chromium Oxide Nanoparticles

Jagriti Behl*, Raksha Saini

Department of Chemistry Sri Sai University, Palampur 176081, Himachal Pradesh, India

*Corresponding authors: E-mail: jagritichem26@gmail.com

DOI: 10.5185/amlett.2021.031613

Mn and Cu-doped Cr_2O_3 nanoparticles were prepared by the co-precipitation method followed by calcination at 400^{0}C for 3h. These synthesized nanoparticles were characterized by Fourier Transform Infrared spectroscopy (FTIR), X-ray Diffraction (XRD), Scanning electron microscope (SEM), Energy-dispersive X-ray spectroscopy, and UV/Visible spectroscopy. SEM images showed the irregular and nearly spherical structure of the Undoped and doped Cr_2O_3 nanoparticles respectively. The particle size of obtained nanoparticles exhibits in the range of 30-60 nm. X-ray diffraction study reveals at temperature 400^{0}C, undoped and Cu-doped Cr_2O_3 nanoparticles exist in the crystalline phase and Mn-doped Cr_2O_3 nanoparticles exist in the amorphous phase. UV-Visible spectra have been used to determine the band gap of the synthesized nanoparticles. The optical band gap value has been calculated by using Tauc's method and Kubelka Munk method. Results indicate band gap calculated by Kubelka-Munk method is higher (4.7, 4.5 and 4.32 eV) than Tauc's method. (4.18, 4.0, 3.96 eV). It is also concluded the decrease in the band gap (in both Tauc's and Kubelka Munk method) was observed by the addition of dopant.

Introduction

In recent years synthesis and characterization of nanoparticles of transition metal oxides attract more attention, because of their unique properties and tremendous applications [**1-3**]. At present, chromium oxide nanoparticles are considered one of the interesting metal oxide materials because they have potential application provinces such as dye and green pigments [**4**], catalysts [**5,6**], hydrogen storage [**7**], protective coating material for thermal protection [**8,9**], Solar collectors [**10,11**], gas and humidity sensor [**12,13**], Cr_2O_3 is an essential material because of its high melting point and high-temperature resistance [**14**]. Composites of Cr_2O_3/ Carbon act as anode material for lithium-ion batteries [**15**], p-type semiconductor [**16**]. Besides, the addition of the dopant in metal oxide nanoparticles results in the formation of composites and improves the properties of metal oxide nanoparticles [**17**]. Therefore it is important to synthesize chromium oxide nanoparticles with and without doping.

In literature, several synthetic techniques for the synthesis of metal oxide nanoparticles are described, including sonochemical synthesis [**18**], hydrothermal [**19**], sol-gel [**20**], laser-induced [**21**], Microwave [**22,23**], and co-precipitation [**24,25**] Among these methods, the co-precipitation method is of great interest because it is cost-effective, and simple method [**26**]. In the present study, a simple co-precipitation method for the synthesis of undoped and doped Cr_2O_3 nanoparticles has been adopted. The main purpose of the present work is to study the effect of doping on the structural and optical properties of chromium oxide nanoparticles.

Experimental

Material and physical measurements

All chemicals used in this work are of the analytical grade and have been used without any further purification. The synthesized chromium oxides nanoparticles were characterized by powder X-ray diffraction using Rigaku X-ray diffractometer with Cu-Kα radiation source (wavelength λ = 1.54060Å) in the range of 10° – 80°. The samples were functionally characterized by Fourier Transform Infrared spectroscopy using FTIR L1600312 spectrum TWOLITA/ZnSe from (AGILENT technology) in the range of 4000-400 cm^{-1}. UV-Vis spectra of the synthesized nanoparticles were recorded in UV-Vis-NIR Spectrophotometer (Perkin Elmer UV-2450). The morphology of the nanoparticles was determined by using a Field emission scanning electron microscope (FESEM) Nova Nano SEM-450, with a carbon coating.

Preparation of chromium oxide nanoparticles

Chromium oxide nanoparticles were synthesized through the co-precipitation method by mixing chromium (III) chloride (0.1M) dissolved in 100 mL of water and Sodium dodecyl sulfate (SDS) (0.1 M in 100 mL water) as a capping agent with constant stirring, then add an aqueous solution of sodium hydroxide (0.1 M in 100 mL) dropwise with continuous stirring for 4h. The green precipitate was filtered and dried in an oven at 50 ^{o}C for 1 h. The obtained

precipitates were calcined in a muffle furnace at 400 °C for 3 h.

Preparation of manganese doped chromium oxide nanoparticles

A homogeneous solution of Cr^{3+} and Mn^{2+} was obtained by mixing an appropriate amount of $CrCl_3.6H_2O$ (0.4M) in 100 mL water and sodium dodecyl sulfate in distilled water. The aqueous solution of the $MnCl_2.4H_2O$ (0.2M in 100 mL) and sodium hydroxide (0.1 M in 100 mL) was added to the above solution with continuous stirring till the pH 10 was reached. After stirring at 50 °C for 3 h, the product was aged for 24 h and the resulting precipitates were centrifuged, followed by washing with distilled water and the ethanol. The sample was then dried at 80 °C for 2 h and the obtained sample was further calcined at 400°C for 3h. Similarly, copper doped Cr_2O_3 nanoparticles were synthesized in an appropriate stoichiometric amount.

Result and discussion

Infrared spectroscopy

The characteristic peaks exhibited by the FTIR spectra of chromium oxide and Mn and Cu-doped chromium oxide nanoparticles are shown in **Fig. 1(a), Fig. 1(b)** and **Fig. 1(c)**. The strong peak at 1090 cm^{-1} and 1062 cm^{-1} in chromium oxide and Mn-doped chromium oxide nanoparticles respectively are assigned to O-H bending vibration, may be due to the presence of adsorption of atmospheric water content [**27**]. Absorption bands observed in the range of 400-680 cm^{-1} are assigned to the stretching modes of M-O bond [**28**]. In chromium oxide nanoparticles a weak band at 672 and 591cm^{-1} are assigned to the Cr-O stretching mode. In Mn-doped Cr_2O_3 oxide nanoparticles a strong and broadband at 542 cm^{-1} assigned for M-O bond (**Fig. 1(b)**). Similarly, broadband at 534 cm^{-1} assigned for M-O bond vibration frequency in Cu-doped Cr_2O_3 nanoparticles. The shift in the frequency in lower reason is due to the change in the microstructured features by the addition of dopant into the Cr-O lattice.

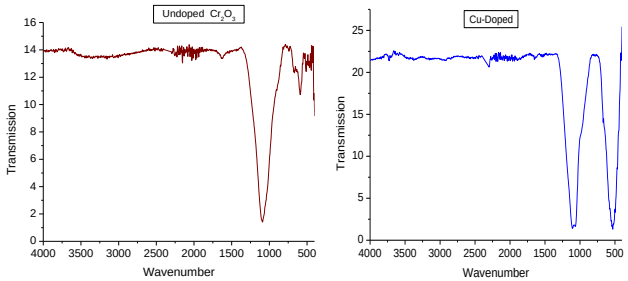

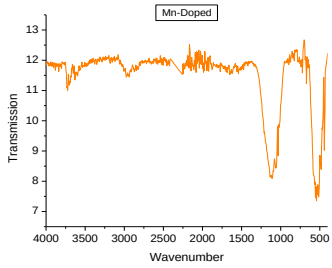

Fig. 1. Infrared spectra of a) undoped Cr_2O_3 (b) Cu-doped Cr_2O_3 and (c) Mn-doped Cr_2O_3 nanoparticles.

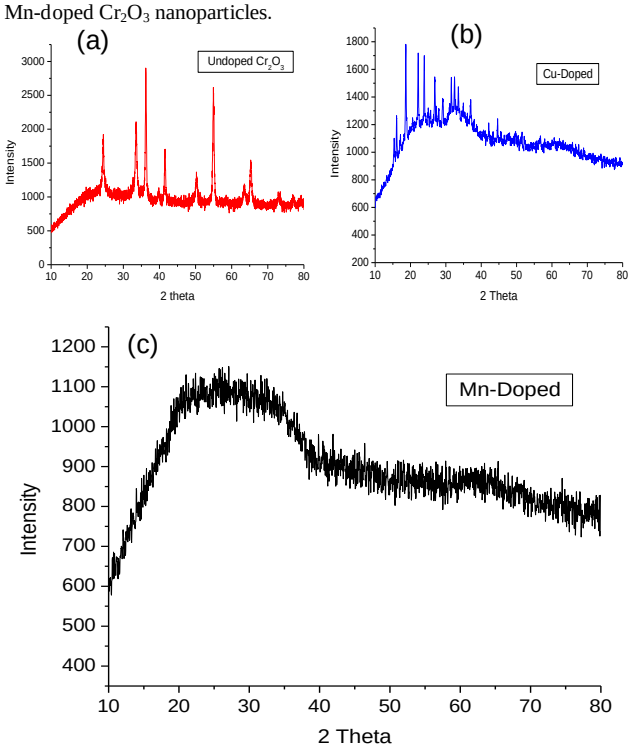

Fig. 2. X-ray diffraction pattern of (a) undoped Cr_2O_3 (match with 072-3533 JCPDS Card), (b) Cu-doped Cr_2O_3 and (c) Mn-doped Cr_2O_3 nanoparticles.

Powder X-Ray diffraction

X-ray diffraction pattern of synthesized undoped and doped Cr_2O_3 nanoparticles is depicted in **Fig. 2**. X-ray diffraction pattern of the undoped chromium oxide nanoparticles matches with previously reported Cr_2O_3 (072-3533 JCPDS Card) [**29,30**]. The high intensity of the peaks indicates the good crystalline nature of the nanoparticles. Cu-doped Cr_2O_3 nanoparticles show crystalline peaks with a shift in 2 theta value (**Fig. 2(b)**) while the X-ray diffraction pattern of the Mn-doped Cr_2O_3 nanoparticles appears to be amorphous (**Fig. 2(c)**), Literature indicates [**31,32**] there exists a temperature range where crystalline and amorphous phases coexist. So with XRD data, it cannot be decided, whether in the Mn-doped Cr_2O_3 nanoparticles are composed of crystalline, amorphous, or both phases. It may be due to the resonant states between which the major optical transition occurs exist both in the amorphous and crystalline phase [**33**] and

there should be little change to the relative amount of the crystalline phase before incubation [**34**].

Morphology

SEM images of the undoped and doped chromium oxide nanoparticles are shown in **Fig. 3**. SEM image **Fig. 3(a)**, indicate Cr_2O_3 nanoparticles are irregular in shape, highly agglomerated, and arranged in layers. On the other hand, Cu and Mn-doped Cr_2O_3 nanoparticles are nearly spherical and agglomerated. However, agglomeration is due to the high surface energy of metal oxide particles that occurs when prepared in an aqueous medium and also possible due to densification resulting in space between particles [**35**]. The particle size of Cr_2O_3 was decreased proportionally by doping. Particle size between 30-60 nm can be seen (**Fig. 3(b) and Fig. 3(c)**).

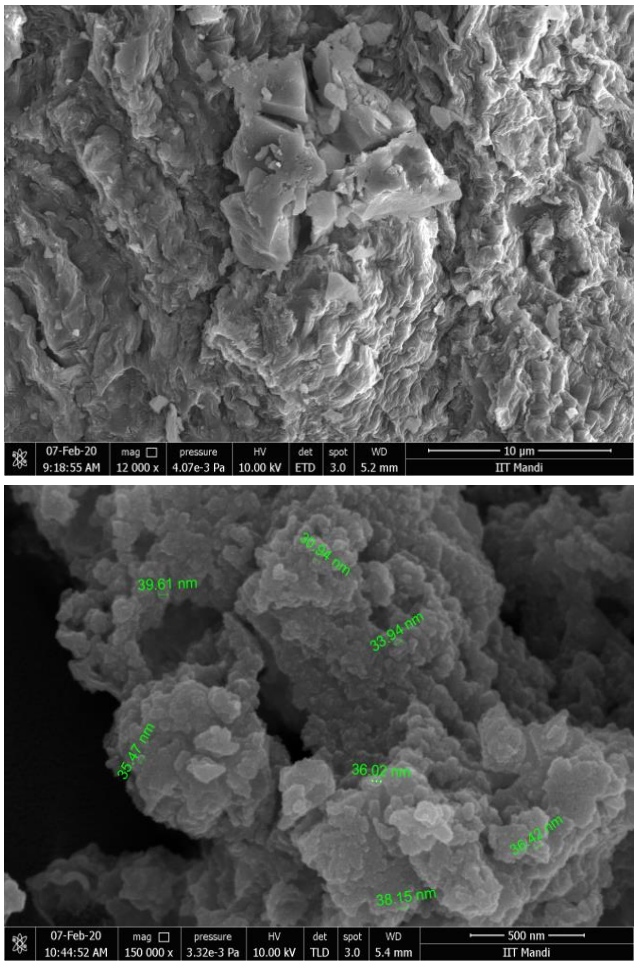

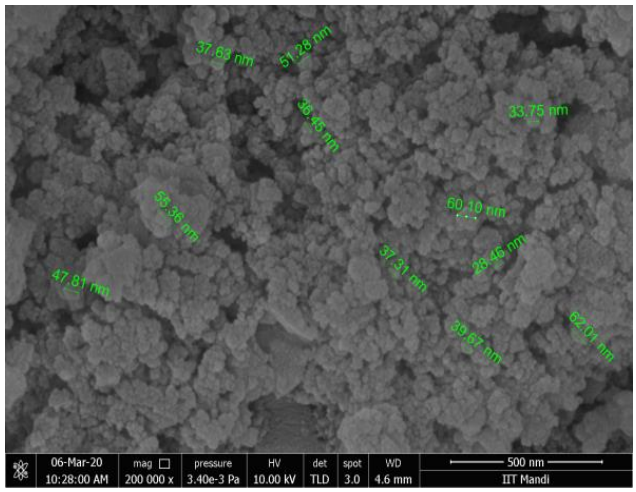

Fig. 3. FESEM images of (a) undoped Cr_2O_3 (b) Cu-doped Cr_2O_3 and (c) Mn-doped Cr_2O_3 nanoparticles.

The EDAX spectra of doped and undoped Cr_2O_3 nanoparticles revealed the presence of Cr, Cu, and O in the sample as shown in Fig. S1 given in supporting material.

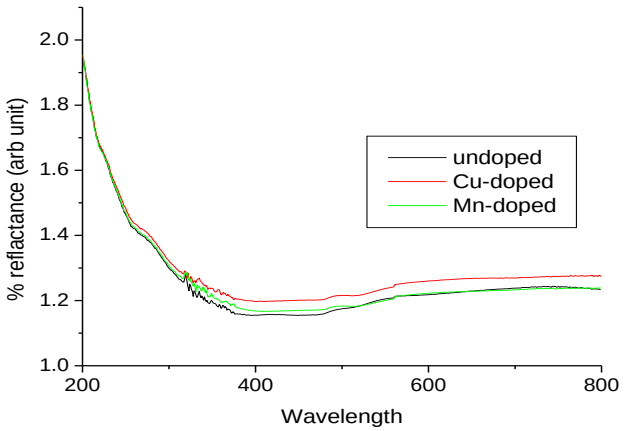

Fig. 4. Diffuse reflectance spectra of Doped and undoped Cr_2O_3 nanoparticles.

Optical properties

The optical properties of undoped and doped Cr_2O_3 nanoparticles were investigated using diffuse reflectance spectroscopy. **Fig. 4.** shows the diffuse reflectance spectra of undoped and Mn and Cu -doped Cr_2O_3 nanoparticles. All samples show absorption in the visible region (460-500 nm) which is a characteristic peak of Cr_2O_3 nanoparticles [**36,37**]. In Cu-doped Cr_2O_3 nanoparticles, absorption peak at 272 nm confirmed the presence of Cu^{2+} ion [**38**].

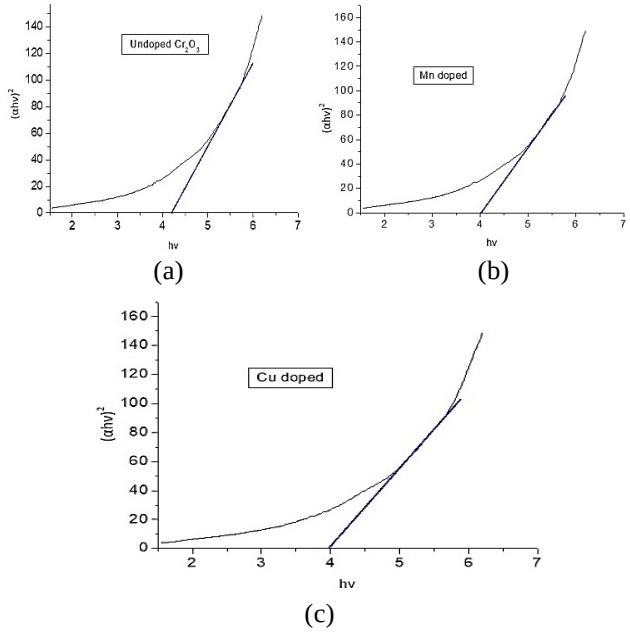

Fig. 5. Tauc's plot of (a) Cr_2O_3 nanoparticles (b) Cu-doped Cr_2O_3 nanoparticles (c) Mn-doped Cr_2O_3 nanoparticles.

The optical band gap energy of the undoped and doped Cr_2O_3 nanoparticles was determined by using the Tauc's equation [**39**] and Kubelka-Munk (KM) method [**40**]. The spectra have shown in **Fig. 5** and **Fig. 6** are given a plot of Tauc's and Kubelka- Munk function. When we use Tauc's equation we obtain Eg = 4.18, 4.0, and 3.96

S. NO	Eg in eV (Tauc's method)	Eg in eV (K-M method)
Undoped Cr_2O_3	4.18	4.7
Mn-doped	4.0	4.5
Cu-doped	3.96	4.32

eV for Cr_2O_3, Mn-doped, and Cu doped Cr_2O_3 respectively. When the Kubelka-Munk equation use, we obtain Eg = 4.7, 4.5, and 4.33eV for Cr_2O_3, Mn-doped, and Cu-doped Cr_2O_3 nanoparticles. The results indicate an increase in band gap value calculated by using the Kubelka-Munk method as compared to Tauc's method. It may be due to, the reflectance of the sample depends on the ratio of absorption coefficient (K) and scattering coefficient (s). When the particle size decreases the scattering coefficient increases and reflectance increases [**41**]. Furthermore, it has been also observed that the energy band gap decreases with the addition of Mn^{2+} and Cu^{2+} ions in both cases (see **Table 1**). The reduction of the band provides further evidence of doping Mn^{2+} and Cu^{2+} ions. From the band gap value it is also evident that Mn^{2+} and Cu^{2+} ions do not occupy the proper substitutional lattice sites to increase free electrons, but causing a decrease of the free electrons [**42**], change in lattice constant by adding dopant [**43**]. From these band gap values, we can conclude that the synthesized undoped and doped Cr_2O_3 nanoparticles act as semiconductors and may find future application in the field of optical electronics devices.

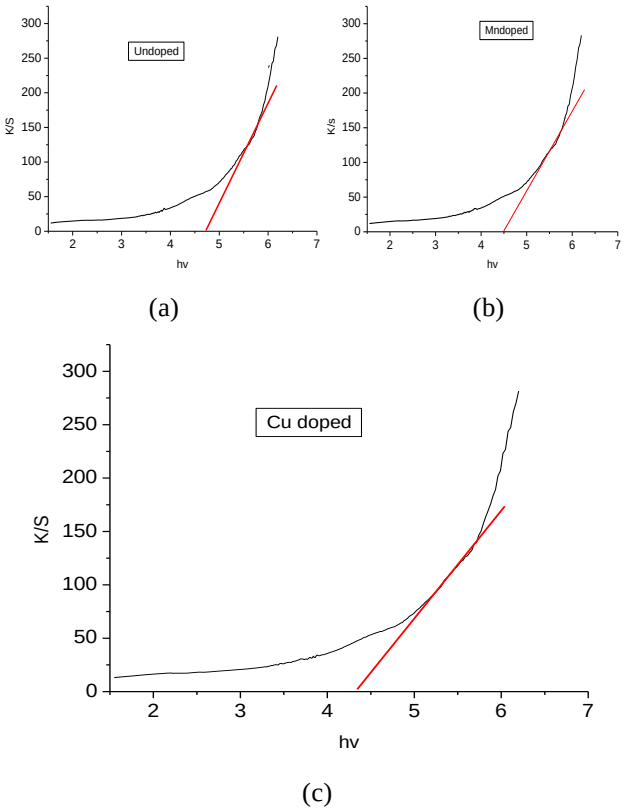

Fig. 6. Kubelka-Munck plot of (a) Cr_2O_3 nanoparticles (b) Cu-doped Cr_2O_3 nanoparticles (c) Mn-doped Cr_2O_3 nanoparticles.

Table 1. Band gap value of undoped and doped Cr_2O_3 nanoparticles.

Conclusion

Undoped and doped Cr_2O_3 nanoparticles were synthesized by co-precipitation method followed by calcination at 400 °C for 3 h and characterized by UV-Vis, IR, and XRD. The morphology and size of the nanoparticles were confirmed by FESEM. The average particle size of the synthesized nanoparticles is in the range of 30-60 nm. The effect of doping on structural and optical properties has been studied. X-ray diffraction study shows at temperature 400°C undoped and Cu-doped Cr_2O_3 nanoparticles exist in the crystalline phase and Mn-doped Cr_2O_3 nanoparticles exist in the amorphous phase. The optical properties of synthesized nanoparticles were studied by using Tauc's method and the Kubelka-Munk method and results indicate the optical band gap calculated by the Kubelka-Munk method is higher band gap as compared to the band gap calculated by Tauc's method. Furthermore, a reduction in the band gap is obtained by the addition of Mn^{2+} and Cu^{2+} ions. It was also concluded that these nanoparticles may be find applications in the field of electronics.

Acknowledgment

The authors are thankful to the AMRC Indian Institute of Technology, Mandi Himachal Pradesh for instrumentation.

Keywords

Band gap studies, co precipitation method, mn-doped chromium oxide, cu-doped chromium oxide, nanoparticles, km method.

Received: 05 June 2020
Revised: 15 June 2020
Accepted: 22 September 2020

References

1. Agnieszka, K. R.; Teofil, J.; *Materials*, **2014**, *7*, 2833.
2. Figueiredo, B. C.; Hyoung, J.K.; Zucolotto, V.; Fuchs, H.; Riehemann.; *Artif. Cell. Nanomed B.*, **2018**, *46*, 694.
3. Riddhiman, M.; Maria, D. M.; Randall, T. Lee.; *ACS Appl. Nano Mater.*, **2020,** *7*, 6156.
4. Sangeetha, S.; Basha R.; Sreeram, K. J.; Sangilimuthu, S.N.; Nair B. U.; *Dyes. Pigm.*, **2012**, *94*, 548.
5. Tanya, T.; Mikaei, J.; Daniela, P.; Momtchil, D.; I van, M.; *Micropor. Mesopor. Mat.*, **2011**, *137*, 56.
6. Nguyen, T. T.; Nguyen Thi, N.; Kuen-Song, L.; *J. Taiwan. Inst. Chem.*, **2018**, 83, 10.
7. Vijay, R.; Sundaresan, R.; Maiya, M.P.; Srinivasa, S. M.; *J. Alloys. Compd.*, **2006,** *424*, 289.
8. Xiaolu, P.; Kewei, G.; Luo, F.; Yusuf, E.; Levin, A. A.; Volinsky, A.A.; TSF., **2009**, *517*, 1922.
9. Monika, D.; Karal, K.; Zbigniew, G., *MTAEC 9*., **2017**, *51*, 603.
10. Rogério, A. X. N.; Vilma, C. C.; Wanger, S.; Frederico, R. A.; Guilherme, M. S.; *Mater. Res.*, **2018**, *21*, e20170556.
11. Khamlich, S.; Nemraoui, O.; Mongwaketsi, N.; Maaza, M.; *Physica B.; Condensed. Matter*, **2012**, *407*, 1509.
12. Xin, G.; Qu, Z.; Zhaorui, Lu.; Lingna, Xu.; Qingyan, Z.; Wen, Z.; *Front. Mater.*, **2019**, Doi. Org/ 10.3389/ fmats.2019.00163.
13. Sajjan, K. C.; Aashis S, R.; Ameena, P.; Syed. K.; *J. Mater Sci-Mater El.*, **2014.**
14. Cellard, A.; Garnier, V.; Fantozzi, G.; Baret, G.; Fort, P.; *Ceram. Int.*, **2009**, *35*, 913.
15. Fu, Ya.; Hongbo, Gu.; Xingru, Y.; Jiurong, Liu.; Yiran, W.; Jiangnan, H.; Xiaoyu, Li.; *Chem. Engin. J.*, **2015**, *277*, 186.
16. Huaqiang, C.; Xianqing, Q.; Yy, L.; Meijuan, Z.; Qiming, Z.; *Appl. Phys. Lett.*, **2006**, *88*, 241112.
17. Sandeep, K. L.; Hsfeez, Y. H.; Pandiyarasan, V.; Ganesh, V.; Anish, K.; Hiroya, I.; Bernowrdshaw, N.; *Appl. Surf. Sci*, **2018**, *449*, 790.
18. Dojalisa, S.; Acharya,, S. B.; Panda, K. A.; *Ultrason. Sonochem.*, **2011**, *18*, 601.
19. Arun, K. J.; Batra, A. K.; Krishna, A.; Bhat, K.; Aggarwal, M.D.; Joseph Francis, P.J.; *Am. J. Mater. Sci.*, **2015**, *5*, 36.
20. Vinod, K.; Singh, R. G.; Purohit, P. L.; Fouran, S., *Adv. Mat, Lett.*, **2013**, *4*, 423.
21. Denis, A. S.; Kristin, R. S.; Thomas, M. O.; *J. Phys. Chem. Lett.*, **2010**, *18*, 2633.
22. Karthik, K.; Dhanuskodi, S.; Gobinath, C.; Prabukumar, S.; Sivaramakrishnan, S.; *J. Mater Sci.: Mater . Elect.*, **2018**, *29*, 5459.
23. Vaishali N, S.; Ratiram G., C.; Ganesh S, B.; Alok R, R.; Harjeet D.; *J. Nano Structure and Nano Objects.*, **2018**, *13*, 121.
24. Jayaprasath, G.; Ravi, G.; Haja, Hameed, A. S.; Mohalingam, T.; *J. Phys. Chem. C.*, **2014**, *118*, 9715.
25. Mahboubeh, H.; Fatemeh, Z.; Zahra, J. R.; Ali, A.; Zohreh, A., *J. Magn. Magn. Mater.*, **2014,** *371*, 43.
26. Haiwen, W.; Xiujuan, Xu.; Jianrong, Z.; Chunzhang, Li.; *J. Mater. Sci. Technol.*, **2010**, *26*, 1037.
27. Nakamoto, K., Infrared and Raman spectra of inorganic and coordination compounds part A and B; John Wiley and Sons, New York, **1997**.
28. Ashiri, R.; *Vib. Spectrosc.*, **2013**, *66*, 24.
29. Gibot, P.; Vidal, L.; *J. Eur. Ceramic. Soc.*, **2010**, *30*, 911.
30. Ahlam, S.; Hadj, B.; Bedhiaf, B.; *High Temp. Mater. Proc.*, **2019**, *38*, 806.
31. Kim, J. H.; Nam, S. K.; Lee, Y. J.; *J. Appl. Phys.*, **1996**, *79*, 1794.
32. Seungbum, H.; Eunah, K.; Dae-Weon, K.; Tae-Hyun, S.; Kwangsoo, No.; *J. Non-Cryst. Solids.*, **1997**, *221*, 245.
33. Zhao, X.; Nomura, S.; Aoyagi, Y.; Sugano, T.; *J. Non-Cryst.. Solids.*, **1996**, *847*, 198.
34. Kinsbron, E.; Sternheim, M.; Knoell, R.; *Appl. Phys. Lett.*, **1983**, *42*, 835.
35. Prashant, B. C.; Ajay, K. P.; Ganesh S. B.; Subhash, S.; Dadamia, PMD. S.; Raghavendra K. M.; Ratiram, G.C.; *Adv. Mater. Lett.*, **2019**, *10*, 355.
36. Ramesh, C.; Mohan, K. K.; Senthil, M.; Ragunathan, V.; *Arch Appl. Sci. Res.*, **2012**, *4*,1894.
37. Quinten, M., Optical properties of nanoparticles systems; Mie and Beyon Wiley VCH Publisher, **2011**.
38. Katwal, R.; Kaur, H.; Sharma, G.; Naushad, Mu.; Pathania, D.; *J. Ind. Eng. Chem.*, **2015**, *31*, 173.
39. Tauc, J.; High Absorption Region, In: J. Tauc (Ed), Amorphous and Liquid Semiconductors, Springer U.S., London and New York **1974**.
40. Kubelka, P.; Munk, F. Z.; *Tech. Phy.*, **1931**, *12*, 593.
41. Jeevanandam, P.; Mulukutha, R. S.; Phillips, M.; Chaudhary, S.; Erickson, L.E.; Klabunde, K.J.; *J. Phys. Chem. C.* **2007**, *111*, 1912.
42. Kelchtermans, A.; Elen, K.; Schellens, K.; Conings, B.; Damn, H.; Boyen, G. H.; Haen, D. J.; Adriaensens, P.; Hardy, H.; Van-Bael, K. M.; *RSC Adv.*, **2013**, *3*, 15254.
43. Motooka, T.; Uda, T.; Handbook of silicon based MEMS materials and technologies (Second Edition), **2015**.